This manuscript was accepted by Appl. Phys. Lett. Click here to see the version of record.

Vacuum Ultraviolet Radiation Effects on Two-Dimensional MoS_2 Field-Effect Transistors

Julian J. McMorrow[1], Cory D. Cress[2], Heather N. Arnold[1], Vinod K. Sangwan[1], Deep Jariwala[1], Scott W. Schmucker[3], Tobin J. Marks[1,4], and Mark C. Hersam[1,4,5]*

[1]Department of Materials Science and Engineering, Northwestern University, Evanston, Illinois 60208, USA

[2]Electronics Science and Technology Division, U.S. Naval Research Laboratory, Washington, D.C. 20375, USA

[3]National Research Council Postdoctoral Associate, U.S. Naval Research Laboratory, Washington, D.C. 20375, USA

[4]Department of Chemistry, Northwestern University, Evanston, Illinois 60208, USA

[5]Department of Electrical Engineering and Computer Science, Northwestern University, Evanston, Illinois 60208, USA

[*]Author to whom correspondence should be addressed. Electronic mail: m-hersam@northwestern.edu

Abstract

Atomically thin MoS_2 has generated intense interest for emerging electronics applications. Its two-dimensional nature and potential for low-power electronics are particularly appealing for space-bound electronics, motivating the need for a fundamental understanding of MoS_2 electronic device response to the space radiation environment. In this Letter, we quantify the response of MoS_2 field-effect transistors (FETs) to vacuum ultraviolet (VUV) total ionizing dose (TID) radiation. Single-layer (SL) and multilayer (ML) MoS_2 FETs are compared to identify differences that arise from thickness and band structure variations. The measured evolution of the FET transport properties are leveraged to identify the nature of VUV-induced trapped charge, isolating the effects of the interface and bulk oxide dielectric. In both the SL and ML cases, oxide trapped holes compete with interface trapped electrons, exhibiting an overall shift toward negative gate bias. Raman spectroscopy shows no variation in the MoS_2 signatures as a result of VUV exposure, eliminating significant crystalline damage or oxidation as possible radiation degradation mechanisms. Overall, this work presents avenues for achieving radiation-hard MoS_2 devices through dielectric engineering that reduces oxide and interface trapped charge.

Manuscript

Molybdenum disulfide (MoS_2) has been the subject of intense research as an n-type two-dimensional channel material for next-generation electronics. MoS_2 field-effect transistors (FETs) exhibit large current on/off ratios (10^8-10^9)[1,2] and sizeable room-temperature field-effect mobilities (30-480 cm^2/Vs),[3-7] which argue that MoS_2 is particularly well-suited for low-power electronics.[8] The MoS_2 electronic band gap, atomic-scale thickness, and strong optical absorption have also attracted interest for vertical heterostructure devices[9-13] and photovoltaic active layers.[14-17] For these reasons as well as proven operation in harsh environments,[18] the unique properties of MoS_2 motivate the study of its suitability as a material in space electronics applications, in which its electronic band gap, large switching ratio, and ultrathin nature are favorable for low-power, light-weight operation. Computational results indicate that within the transition metal dichalcogenides[19] and black phosphorus,[20] MoS_2 is among the least susceptible to radiation-induced defect formation. The exceptionally small cross-sections of MoS_2 flakes are further advantageous for radiation hardness to single-event effects (SEEs),[21] suggesting that the interactions of the surrounding materials with incident radiation in the form of total ionizing dose (TID) will play the greatest role in the radiation response of MoS_2 as a semiconducting electronic device component. Initial studies on the basic mechanisms driving the TID response of MoS_2 field-effect transistors (FETs) have revealed the extrinsic effect of atmospheric adsorbates on the evolution of device transport properties[22] or have demonstrated radiation damage effects that are possibly convoluted with atmospheric adsorbates.[23] Because such atmospheric effects have also been shown to dominate the radiation response of other low-dimensional nanoelectronic systems,[24,25] the radiation response of MoS_2 must be isolated from extrinsic factors to reveal the intrinsic behavior of MoS_2 FETs.

In this Letter, we investigate the vacuum ultraviolet (VUV) TID response of both single-layer (SL) and multilayer (ML) MoS_2 FETs having SiO_2 gate dielectrics under high vacuum. For decades, VUV exposure has been used to understand radiation-induced charge trapping in SiO_2 due to its spatially

This manuscript was accepted by Appl. Phys. Lett. Click here to see the version of record.

shallow absorption near the incident surface and lack of displacement damage in Si or its adjacent oxides.[26-28] Contrary to previous experiments conducted under ambient conditions, it is found that MoS_2 FETs exhibit threshold voltage shifts toward *negative* gate biases under VUV exposure. Furthermore, the evolution of the transport curves as a function of VUV reveals the relative contributions of oxide and interface trapped charge. The maximum drain current and field-effect mobility are observed to increase with increasing dose, which is unique to MoS_2 compared to other two-dimensional electronic materials.[29,30] Finally, Raman spectroscopy before and after VUV exposure reveals no measureable structural changes in the MoS_2 channel, establishing the gate dielectric as the sensitive component of the system and suggesting dielectric engineering as a promising strategy for enhancing the radiation hardness of MoS_2 FETs.

The semiconducting channels of the FETs were prepared by micromechanically exfoliating MoS_2 flakes using the Scotch tape method onto degenerately doped n-type Si substrates having 300 nm thick thermal SiO_2. Single-layer (SL) and multilayer (ML) flakes were identified optically for subsequent device fabrication. Gold source and drain contacts were patterned *via* standard electron-beam lithography, thermal evaporation, and liftoff processes. Figure 1 includes the optical images of the SL and ML devices. The SL MoS_2 channel is outlined in Figure 1(a) and has dimensions of 2.9 μm × 6.8 μm (L × W), while the ML channel in Figure 1(b) is 3.1 μm × 6.3 μm, the width of the latter being the average of its trapezoidal bases. Electrical contacts were deposited without an adhesion layer to facilitate quasi-ohmic contact to the MoS_2 channel.[4] The Si substrate functions as a global back gate contact for three-terminal FET devices, and the fabricated samples were wire-bonded to a ceramic package to allow *in situ* measurements under vacuum. A device schematic of a SL device is depicted in Figure 1(c). The ML channel device in this study consists of a van der Waals stack of six MoS_2 layers as determined by Raman spectroscopy (Supplementary Figure S1). Additional fabrication details were published previously.[31]

The evolution of the electronic transport characteristics of the SL and ML MoS_2 FET devices were measured as a function of sequentially larger VUV doses at pressures below 10^{-6} Torr and under a photon

This manuscript was accepted by Appl. Phys. Lett. Click here to see the version of record.

flux of 3.4×10^{10} photons/cm^{2}s. This flux includes only those photons having energies large enough to be absorbed by the SiO_2 ($E_g \geq 9$ eV). A calibrated silicon photodiode with enhanced extreme and vacuum ultraviolet responsivity (AXUV100G, Opto Diode) was used to quantify the irradiance of the vacuum ultraviolet light source (L10366 series, Hamamatsu Photonics K.K.). This quantification was performed by measuring the photocurrent at the sample position and converting it to irradiance (0.58 μW/cm^2) based on the calibrated photodiode responsivity and VUV bulb spectrum. I_d-V_g transport measurements were carried out before irradiation and after each VUV exposure. During VUV exposure, the devices were held at a constant drain bias (5 mV) and constant forward gate bias (+1 MV/cm) to facilitate separation and collection of VUV-liberated charge carriers in the dielectric. *In situ* measurements are critical to gauging the radiation response of these unencapsulated devices in the absence of atmospheric adsorbates. All measurements and exposures were performed at room temperature. The linear field-effect mobilities for the as-fabricated SL and ML devices were found to be 6.4 cm^2/Vs and 42 cm^2/Vs, respectively. The I_d-V_g curves prior to VUV exposure for both devices are included in black in Figure 2. The accumulated VUV dose has the effect of increasing the maximum drain current and subthreshold swing while shifting the transfer characteristics toward negative gate bias (red curves). The shift toward negative gate bias for both devices indicates an overall accumulation of positive charge between the MoS_2 channel and the gate electrode.

Analysis of the collective changes in threshold voltage and subthreshold swing can be used to quantify the number and type of VUV-induced trapped charges in the MoS_2-SiO_2 FET. These trapped charges are expected to be located predominantly within the gate oxide layer or at the MoS_2-SiO_2 interface. Effects related to surface adsorbates or top-surface interface charges are not considered because these devices are not encapsulated by dielectric layers and the irradiations are performed under vacuum. The observed shift in threshold voltage, ΔV_{th}, is given by separate contributions from oxide trapped charges and interface trapped charges, ΔV_{OT} and ΔV_{IT}, respectively. For a given VUV dose, the net effect is $\Delta V_{th} = \Delta V_{OT} + \Delta V_{IT}$.[32] For two states having different subthreshold swings (*i.e.*, before and

This manuscript was accepted by Appl. Phys. Lett. Click here to see the version of record.

after exposure), the induced interface trapped charge, ΔN_{IT}, is computed as $\Delta N_{IT} = \frac{C_{ox}}{\ln 10}\frac{\phi_b}{kT}\Delta SS$, where ΔSS is the observed difference in subthreshold swings. At room temperature, kT = 26 meV and ϕ_b is the energy difference between the midgap energy and the Fermi level, 0.4 eV and 0.15 eV for the SL and ML devices, respectively.[33] Given ΔN_{IT}, the corresponding ΔV_{IT} is computed from $\Delta V_{IT} = \frac{q}{C_{ox}}\Delta N_{IT}$.

The values of ΔV_{th}, ΔV_{OT}, and ΔV_{IT} are computed for each VUV dose and are plotted as a function of dose for both devices in Figure 3. Due to the biasing conditions during irradiation (+1 MV/cm across the SiO_2 gate dielectric), holes liberated by incident photons will migrate toward the MoS_2-SiO_2 interface, where they are trapped in defect centers known to exist in SiO_2.[34] Additionally, the positive gate bias brings the MoS_2 channel into accumulation, where the large electron density can supply electrons to fill energetically favorable interface states. Thus, we assign the signs of ΔV_{OT} and ΔV_{IT} to be positive and negative, respectively. For a total VUV dose of 2.2 x 10^{13} photons/cm^2, we observe that ΔV_{OT} and ΔV_{IT} shift in opposite directions, which is the net effect of hole trapping in the bulk SiO_2 (shifts toward negative gate bias) and electron trapping at the MoS_2-SiO_2 interface (shifts toward positive gate bias). The overall effect is a comparatively small magnitude shift toward negative gate bias.

While the qualitative similarity of the trends in the charge trapping and voltage shifts in the present SL and ML devices suggest similar mechanisms affecting transport in both devices, the magnitudes and behaviors are quantifiably different. The maximum values of ΔV_{OT} and ΔV_{IT} for the SL device (-54 V and 41 V, respectively) are significantly larger than the ML device (-30 V and 16 V), an observation that is explained by the larger electronic transport band gap and reduced screening in single-layer MoS_2 *versus* multilayer MoS_2 (E_g = 2.7 – 2.8 eV and 1.3 eV, respectively[33,35]). The larger transport band gap is reflected in the ϕ_b term in ΔN_{IT}, allowing a higher quantity of trap states, and thus larger voltage shifts. While the voltage shifts in the ML device (Figure 3(b)) occur monotonically as a function of dose, the SL device (Figure 3(a)) exhibits ΔV_{OT} and ΔV_{IT} values that vary without an identifiable trend until the high dose regime is reached (> 10^{13} photons/cm^2). This variability might arise from the "all-surface" nature of SL MoS_2, where current is strictly confined within the two-dimensional plane. The ML device also has a

This manuscript was accepted by Appl. Phys. Lett. Click here to see the version of record.

thickness comparable to the Debye length of 7 nm in ML MoS_2, suggesting its current flow hot spot is removed from the MoS_2-SiO_2 interface.[36] The result is that charged substrate or adsorbate impurities are less effectively screened from the electronic channel in the SL device, an effect illustrated by the superlinear dependence of the drain current on the gate voltage in the transfer characteristics of the SL device compared to the ML device (Figure 2).[37] Additionally, the SL device exhibits larger fluctuations with charge redistribution under low radiation doses and stronger voltage shifts at higher doses.

In addition to the increase in maximum current, the field-effect mobility ($\mu_{FE} \sim \frac{\partial I_d}{\partial V_g}$) is enhanced as a function of VUV dose for both devices. The changes in field-effect mobility relative to the pre-radiation values as a function of VUV dose for the SL and ML devices are shown in Figures 3(c) and 3(d), respectively. This trend stands in contrast to graphene FETs on SiO_2 gate dielectrics, which suffer significant mobility degradation on radiation exposure as a result of Coulomb scattering induced by dielectric trapped charges. For MoS_2 FETs, the increased field-effect mobility with increased oxide and interface-trapped charge indicates a transport mechanism that is not dominated by Coulomb scattering at room temperature. This conclusion is consistent with previous studies that showed phonon scattering limited transport at room temperature for MoS_2 FETs.[4] Additionally, the increased field-effect mobility is the opposite of what is observed in MoS_2 devices exposed to X-ray[22] and proton irradiation[23] under ambient conditions, emphasizing the importance of controlling the atmosphere during MoS_2 radiation studies. This observation is consistent with those for other low-dimensional electronic systems, such as carbon nanotubes[24] and graphene[25], in which fundamentally different electronic responses are measured when irradiating under vacuum and ambient conditions. Finally, chemisorbed oxygen or the formation of insulating MoO_x species would be expected to decrease device field-effect mobility and maximum drain current, neither of which is observed.

Raman spectroscopy was next used to further investigate the structural evolution of MoS_2 as a result of VUV exposure. The Raman spectra of MoS_2 flakes have been extensively studied, and important structural data such as layer number[38] and oxidation content[39] are readily identified by characteristic

This manuscript was accepted by Appl. Phys. Lett. Click here to see the version of record.

positions of the Raman peaks corresponding to the E^1_{2g} and A_{1g} vibrational modes. Figure 4 shows the Raman spectra and spatial maps of a MoS_2 flake having multiple thickness regions before and after VUV exposure for 640 s. An optical image of this MoS_2 flake is provided in Figure 4(a). Raman spectra (532 nm excitation) are captured and peaks are fit to Lorentzian functions. Figure 4(b) includes pre-exposure and post-exposure Raman maps of the peak separation of the MoS_2 E^1_{2g} and A_{1g} vibrational modes, a quantity known to vary with MoS_2 layer number[40] and chemisorbed oxygen.[39] A comparison of the before and after Raman maps reveals no significant variation as a result of VUV exposure. Choosing isolated regions, the Raman spectra are shown for bulk-like (spot 1), 4-layer (spot 2), and 3-layer (spot 3) MoS_2 in Figure 4(c). Comparing these spectra before and after VUV exposure corroborates that the Raman signature of MoS_2 does not change with VUV dose for a range of flake thicknesses. This lack of significant structural changes in the MoS_2 channel indicates that the changes in electronic transport induced by VUV exposure are dominated by charge trapping in the SiO_2 and at the MoS_2-SiO_2 interface, rather than by severe damage to the MoS_2 crystal structure. These observations are consistent with TID experiments in other low-dimensional nanoelectronic systems such as graphene[29] and carbon nanotube[24] FETs.

In summary, this work delineates and quantifies the charge trapping behavior intrinsic to the MoS_2-SiO_2 system in the absence of atmospheric adsorbates following exposure to VUV radiation. Electronic transport characteristics are found to shift toward negative gate bias, consistent with the trapping of TID-generated holes known to occur in SiO_2. Additionally, a significant quantity of negative charge is trapped at the MoS_2-SiO_2 interface, and the field-effect mobility is found to increase with VUV exposure. The shift toward negative gate bias and increase in mobility with increasing radiation dose are observations that contradict earlier studies and can be attributed to the isolation of the MoS_2 FET from ambient exposure during irradiation. Finally, Raman spectroscopy data indicate no major structural changes or oxidation of the MoS_2 with VUV dose, suggesting the interaction of TID with the MoS_2-SiO_2 system occurs primarily within the oxide layer. The similarity of the charge trapping behavior in the MoS_2-SiO_2

This manuscript was accepted by Appl. Phys. Lett. Click here to see the version of record.

system compared to conventional Si-SiO_2 devices indicates that dielectric-based TID hardening strategies as employed in Si[34] and other nanomaterial[41,42] electronics should be applicable to two-dimensional MoS_2.

Supplementary Material

See supplementary material for Raman characterization of the multilayer MoS_2 FET.

Acknowledgements

This work was supported by the MRSEC program of the National Science Foundation (DMR-1121262), the National Aeronautics and Space Administration NSTRF Grants NNX12AM44H and NNX11AM87H, and the Defense Threat Reduction Agency (MIPR #HDTRA-15-15399). V.K.S. acknowledges support from the 2-DARE Program (NSF EFRI-1433510). This research was performed while S.W.S. held a National Research Council Associateship Award at the U.S. Naval Research Laboratory. This work made use of the EPIC, Keck-II, and SPID facilities of Northwestern University NU*ANCE* Center, which has received support from the Soft and Hybrid Nanotechnology Experimental (SHyNE) Resource (NSF NNCI-1542205); the MRSEC program (NSF DMR-1121262); the International Institute for Nanotechnology (IIN); the Keck Foundation; and the State of Illinois.

Figures

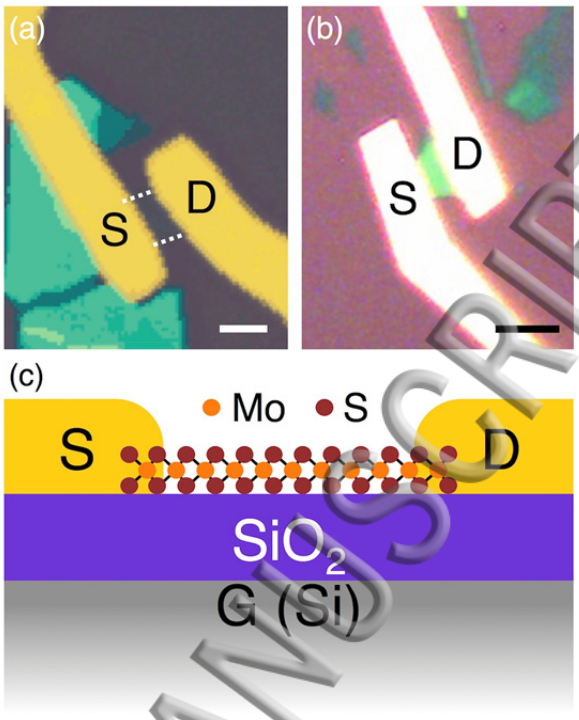

Figure 1. Top view optical images of (a) single-layer and (b) multilayer MoS_2 FET devices with labeled source and drain contacts. The single-layer MoS_2 channel region is highlighted by dotted lines, and the scale bars are 5 μm. (c) Side view schematic of a single-layer MoS_2 FET device, with labeled source and drain contacts, 300 nm thick SiO_2 gate dielectric, and global back gate contact.

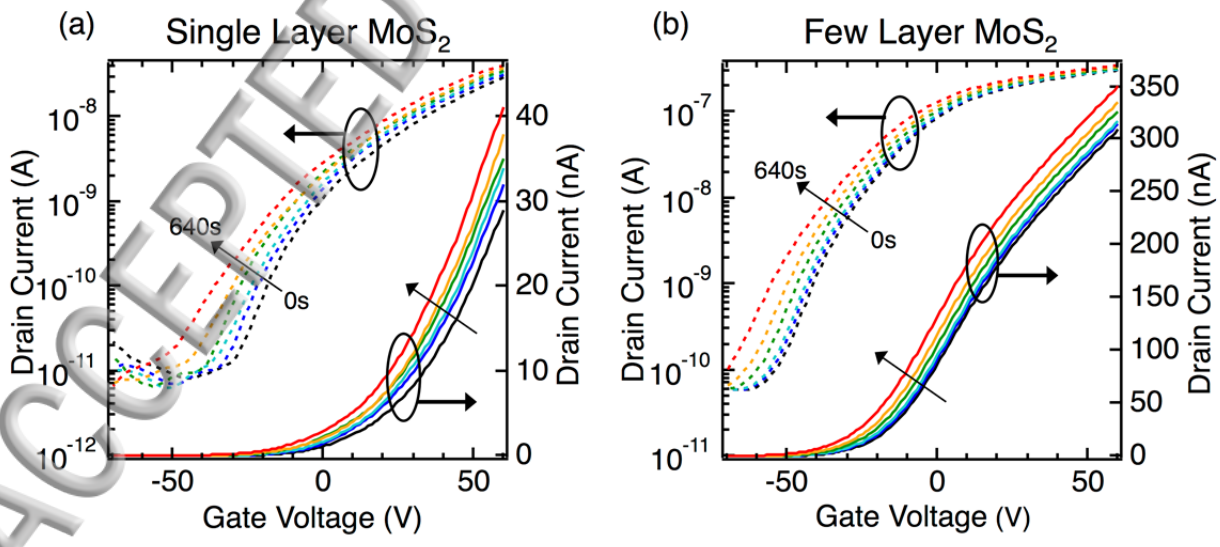

Figure 2. Linear (right axes) and subthreshold (logarithmic, left axes) transport characteristics of single-layer (a) and multilayer (b) MoS_2 FETs as a function of VUV total ionizing dose. Red curves are pre-

This manuscript was accepted by Appl. Phys. Lett. Click here to see the version of record.

radiation transfer plots. The other curves shift toward reverse bias as a function of irradiation for both devices. An increase in subthreshold swing is also observed in both devices.

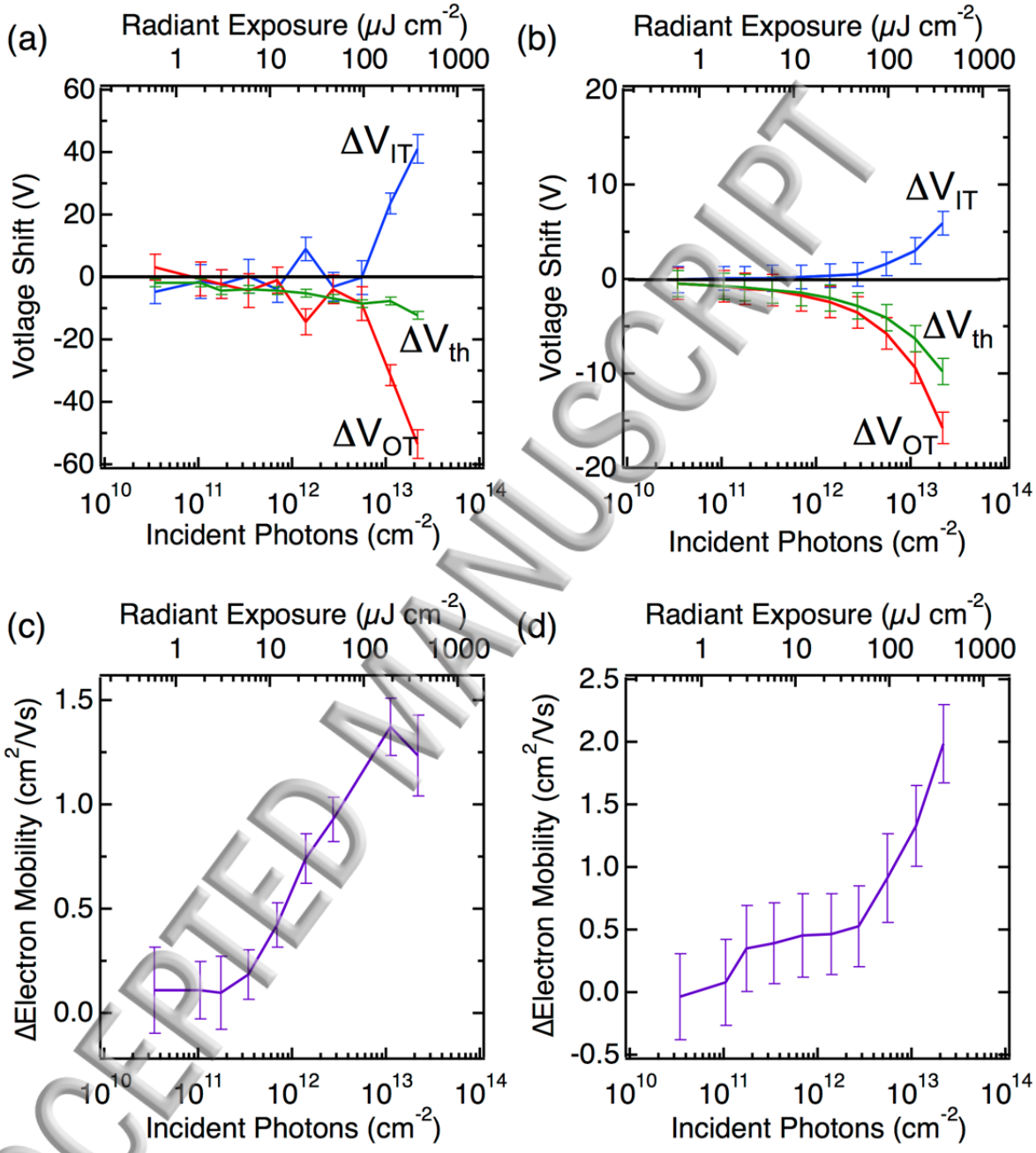

Figure 3. Voltage shifts as a function of VUV dose (incident photons/cm^2) in the (a) single-layer and (b) multilayer MoS_2 devices. Voltage shifts due to interfacial trapped charge (ΔV_{IT}) are shown in blue, threshold voltage shifts (ΔV_{th}) are shown in green, and voltage shifts due to oxide trapped charge (ΔV_{OT}) are shown in red. Error bars for ΔV_{IT} and ΔV_{th} are derived from slope and intercept computations in the I_d -V_g curves. (c) Single-layer and (d) multilayer MoS_2 field-effect mobilities change as a function of VUV dose (incident photons/cm^2), exhibiting an increase in mobility for both devices. Error bars are derived from the computation of the slopes of the I_d -V_g curves.

This manuscript was accepted by Appl. Phys. Lett. Click here to see the version of record.

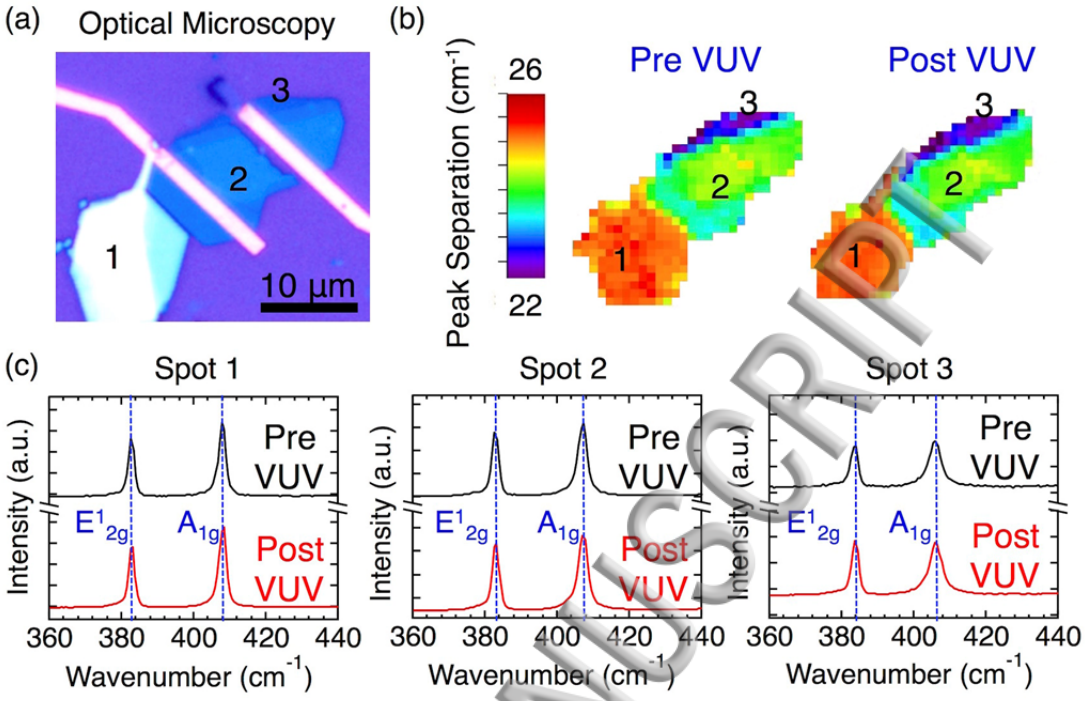

Figure 4. (a) Optical image of the MoS_2 flake for Raman spectroscopy study. (b) Spatial Raman maps depicting the peak separation between the E^1_{2g} and A_{1g} vibrational modes. Three spatial regions corresponding to different layer thicknesses on the MoS_2 flake are identified (spot 1 = bulk-like; spot 2 = 4-layer; spot 3 = 3-layer). (c) Averaged Raman spectra corresponding to points 1, 2, and 3 in (b). The spectra are found to be invariant as a function of VUV dose.

References

[1] H. Liu, A.T. Neal, and P.D. Ye, ACS Nano **6**, 8563 (2012).

[2] W. Wu, D. De, S.-C. Chang, Y. Wang, H. Peng, J. Bao, and S.-S. Pei, Appl. Phys. Lett. **102**, 142106 (2013).

[3] W. Bao, X. Cai, D. Kim, K. Sridhara, and M.S. Fuhrer, Appl. Phys. Lett. **102**, 042104 (2013).

[4] D. Jariwala, V.K. Sangwan, D.J. Late, J.E. Johns, V.P. Dravid, T.J. Marks, L.J. Lauhon, and M.C. Hersam, Appl. Phys. Lett. **102**, 173107 (2013).

[5] N.R. Pradhan, D. Rhodes, Q. Zhang, S. Talapatra, M. Terrones, P.M. Ajayan, and L. Balicas, Appl. Phys. Lett. **102**, 123105 (2013).

[6] H. Schmidt, S. Wang, L. Chu, M. Toh, R. Kumar, W. Zhao, A.H. Castro Neto, J. Martin, S. Adam, B. Özyilmaz, and G. Eda, Nano Lett. **14**, 1909 (2014).

[7] K. Kang, S. Xie, L. Huang, Y. Han, P.Y. Huang, K.F. Mak, C.-J. Kim, D. Muller, and J. Park, Nature

[7] **520**, 656 (2015).

[8] C.U. Kshirsagar, W. Xu, Y. Su, M.C. Robbins, C.H. Kim, and S.J. Koester, ACS Nano **10**, 8457 (2016).

[9] D. Jariwala, V.K. Sangwan, C.-C. Wu, P.L. Prabhumirashi, M.L. Geier, T.J. Marks, L.J. Lauhon, and M.C. Hersam, P. Natl. Acad. Sci. USA **110**, 18076 (2013).

[10] D. Jariwala, S.L. Howell, K.-S. Chen, J. Kang, V.K. Sangwan, S.A. Filippone, R. Turrisi, T.J. Marks, L.J. Lauhon, and M.C. Hersam, Nano Lett. **16**, 497 (2016).

[11] D. Jariwala, V.K. Sangwan, J.-W.T. Seo, W. Xu, J. Smith, C.H. Kim, L.J. Lauhon, T.J. Marks, and M.C. Hersam, Nano Lett. **15**, 416 (2015).

[12] D. Jariwala, V.K. Sangwan, L.J. Lauhon, T.J. Marks, and M.C. Hersam, ACS Nano **8**, 1102 (2014).

[13] A.K. Geim and I.V. Grigorieva, Nature **499**, 419 (2013).

[14] T.A. Shastry, I. Balla, H. Bergeron, S.H. Amsterdam, T.J. Marks, and M.C. Hersam, ACS Nano **10**, 10573 (2016).

[15] S.B. Homan, V.K. Sangwan, I. Balla, H. Bergeron, E.A. Weiss, and M.C. Hersam, Nano Lett. **17**, 164 (2016).

[16] D. Jariwala, A.R. Davoyan, G. Tagliabue, M.C. Sherrott, J. Wong, and H.A. Atwater, Nano Lett. **16**, 5482 (2016).

[17] M. Bernardi, M. Palummo, and J.C. Grossman, Nano Lett. **13**, 3664 (2013).

[18] C. Jiang, S.L. Rumyantsev, R. Samnakay, M.S. Shur, and A.A. Balandin, J. Appl. Phys. **117**, 064301 (2015).

[19] H.-P. Komsa, J. Kotakoski, S. Kurasch, O. Lehtinen, U. Kaiser, and A.V. Krasheninnikov, Phys. Rev. Lett. **109**, 035503 (2012).

[20] V. Vierimaa, A.V. Krasheninnikov, and H.-P. Komsa, Nanoscale **8**, 7949 (2016).

[21] O. Musseau, IEEE Trans. Nucl. Sci. **43**, 603 (1996).

[22] C.X. Zhang, A.K.M. Newaz, B. Wang, E.X. Zhang, G.X. Duan, D.M. Fleetwood, M.L. Alles, R.D. Schrimpf, K.I. Bolotin, and S.T. Pantelides, IEEE Trans. Nucl. Sci. **61**, 2862 (2014).

[23] T.-Y. Kim, K. Cho, W. Park, J. Park, Y. Song, S. Hong, W.-K. Hong, and T. Lee, ACS Nano **8**, 2774 (2014).

[24] C.D. Cress, J.J. McMorrow, J.T. Robinson, A.L. Friedman, and B.J. Landi, IEEE Trans. Nucl. Sci. **57**, 3040 (2010).

[25] C.D. Cress, J.J. McMorrow, J.T. Robinson, B.J. Landi, S.M. Hubbard, and S.R. Messenger, Electronics **1**, 23 (2012).

[26] G.W. Hughes, R.J. Powell, and M.H. Woods, Appl. Phys. Lett. **29**, 377 (1976).

[27] D. J. DiMaria, Z.A. Weinberg, and J.M. Aitken, J. Appl. Phys. **48**, 898 (1977).

[28] S. Scharf, M. Schmidt, F. Wulf and D. Bräunig, IEEE Trans. Nucl. Sci. **41**, 460 (1994).

[29] C.D. Cress, J.G. Champlain, I.S. Esqueda, J.T. Robinson, A.L. Friedman, and J.J. McMorrow, IEEE Trans. Nucl. Sci. **59**, 3045 (2013).

[30] C. Liang, Y. Su, E.X. Zhang, K. Ni, M.L. Alles, R.D. Schrimpf, D.M. Fleetwood, and S.J. Koester, IEEE Trans. Nucl. Sci. DOI: 10.1109/TNS.2016.2616282 (2016).

[31] V.K. Sangwan, H.N. Arnold, D. Jariwala, T.J. Marks, L.J. Lauhon, and M.C. Hersam, Nano Lett. **13**, 4351 (2013).

[32] P.J. McWhorter and P.S. Winokur, Appl. Phys. Lett. **48**, 133 (1986).

[33] S.L. Howell, D. Jariwala, C.-C. Wu, K.-S. Chen, V.K. Sangwan, J. Kang, T.J. Marks, M.C. Hersam, and L.J. Lauhon, Nano Lett. **15**, 2278 (2015).

[34] T.R. Oldham and F.B. McLean, IEEE Trans. Nucl. Sci. **50**, 483 (2003).

[35] Y. Lin, X. Ling, L. Yu, S. Huang, A.L. Hsu, Y.-H. Lee, J. Kong, M.S. Dresselhaus, and T. Palacios, Nano Lett. **14**, 5569 (2014).

[36] S. Das and J. Appenzeller, Nano Lett. **13**, 3396 (2013).

[37] S. Ghatak, A.N. Pal, and A. Ghosh, ACS Nano **5**, 7707 (2011).

[38] C. Lee, H. Yan, L.E. Brus, T.F. Heinz, J. Hone, and S. Ryu, ACS Nano **4**, 2695 (2010).

[39] W.L. Chow, X. Luo, S.Q. Quek, and B.K. Tay, Adv. Electron. Mater. **1**, 1 (2015).

[40] H. Li, Q. Zhang, C.C.R. Yap, B.K. Tay, T.H.T. Edwin, A. Olivier, and D. Baillargeat, Adv. Funct. Mater. **22**, 1385 (2012).

[41] C.D. Cress, J.J. McMorrow, J.T. Robinson, A.L. Friedman, H.L. Hughes, B.D. Weaver, and B.J. Landi, MRS Commun. **1**, 27 (2011).

[42] H.N. Arnold, C.D. Cress, J.J. McMorrow, S.W. Schmucker, V.K. Sangwan, L. Jaber-Ansari, R. Kumar, K.P. Puntambekar, K.A. Luck, T.J. Marks, and M.C. Hersam, ACS Appl. Mater. Interfaces **8**, 5058 (2016).

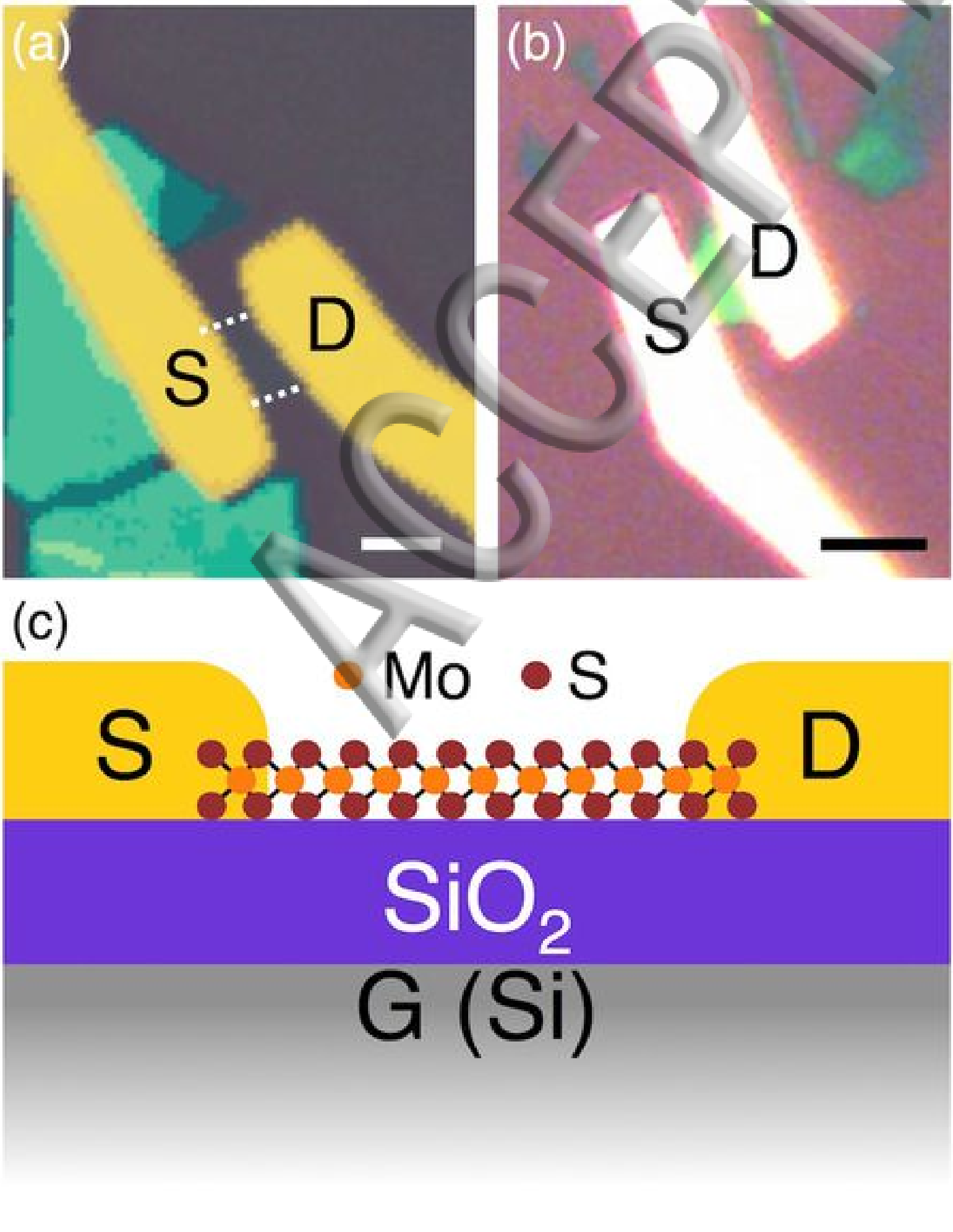
(a)
S
D
(b)
S
D
(c)
Mo
S
S
D
SiO2
G (Si)

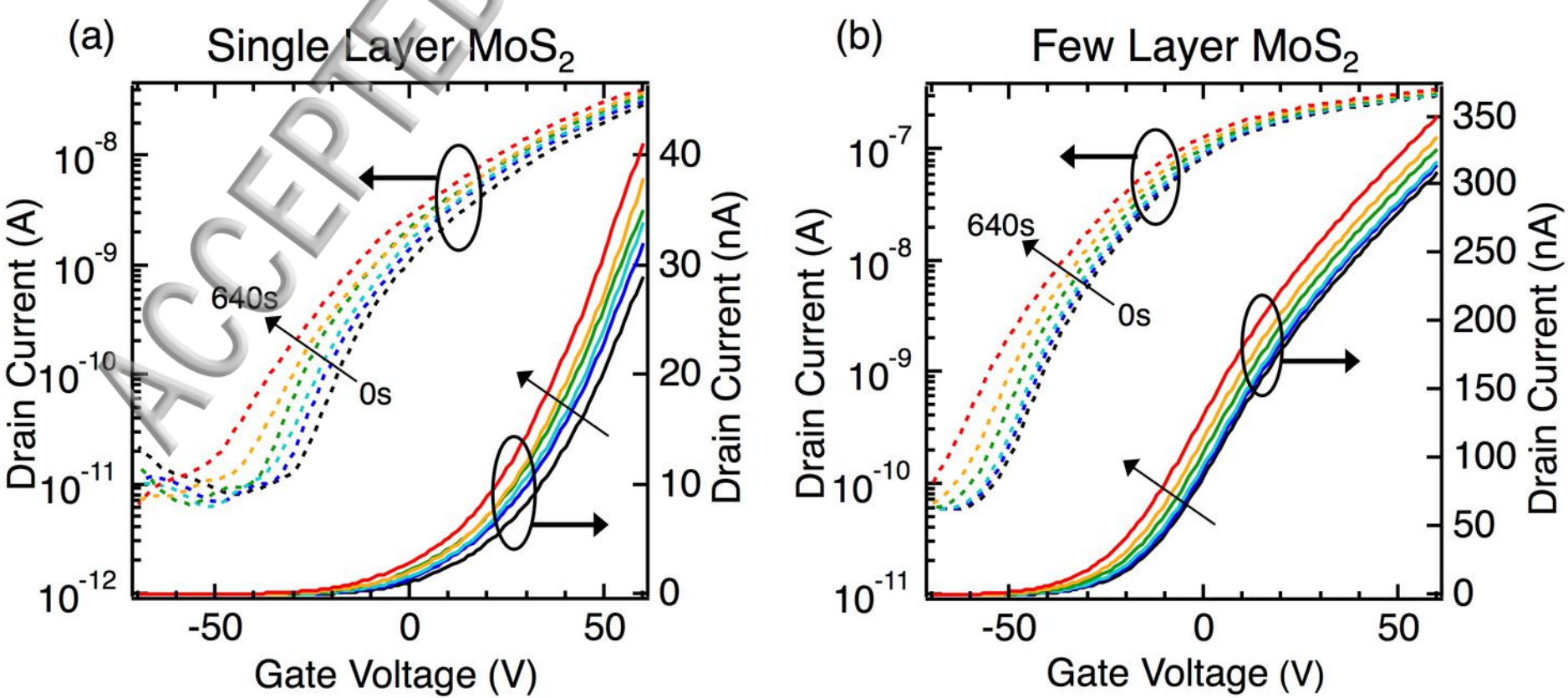
(a)
Single Layer MoS_2
Drain Current (A)
10^{-8}
10^{-9}
10^{-10}
10^{-11}
10^{-12}
640s
0s
Drain Current (nA)
40
30
20
10
0
-50
0
50
Gate Voltage (V)
(b)
Few Layer MoS_2
Drain Current (A)
10^{-7}
10^{-8}
10^{-9}
10^{-10}
10^{-11}
640s
0s
Drain Current (nA)
350
300
250
200
150
100
50
0
-50
0
50
Gate Voltage (V)

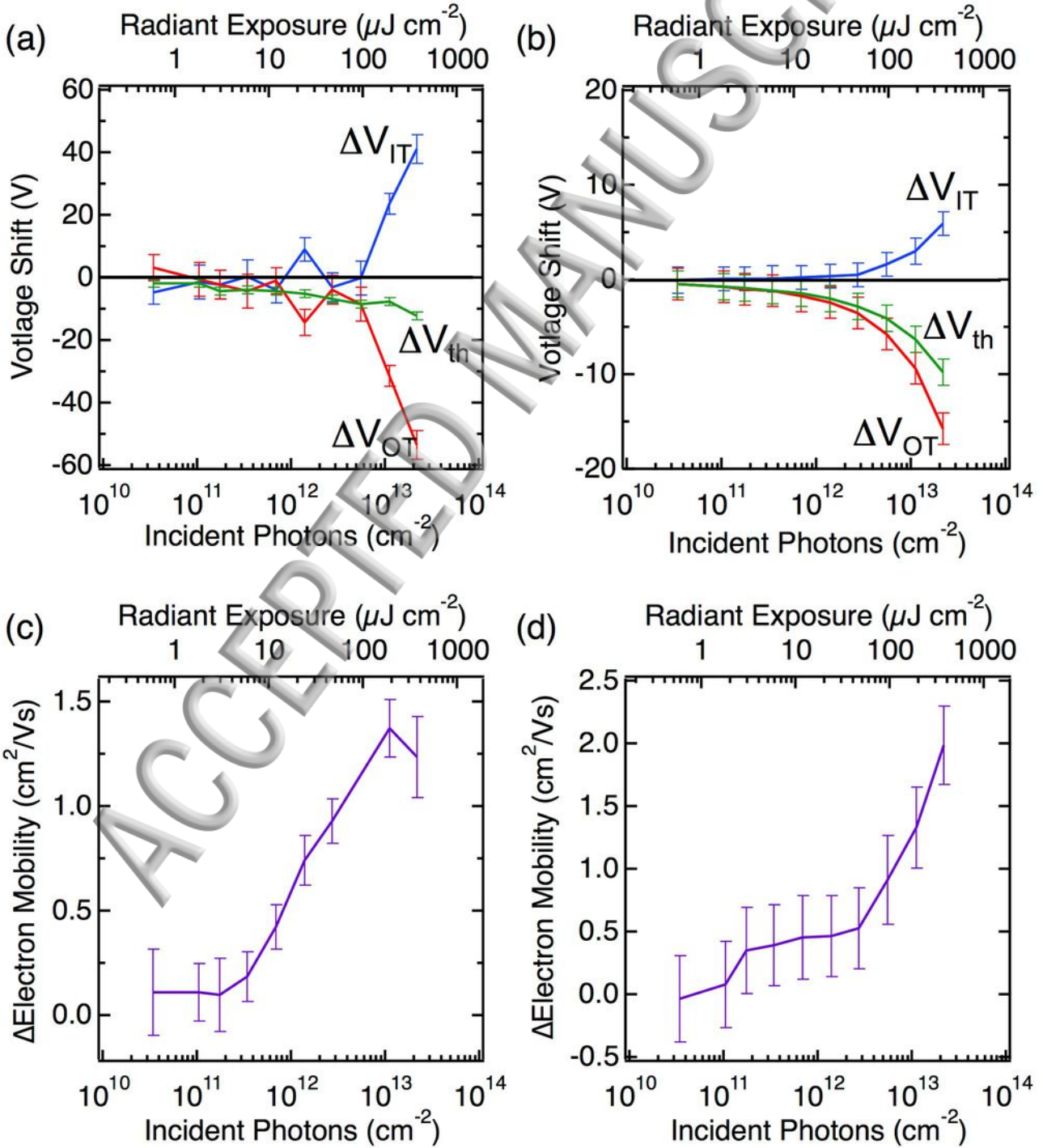

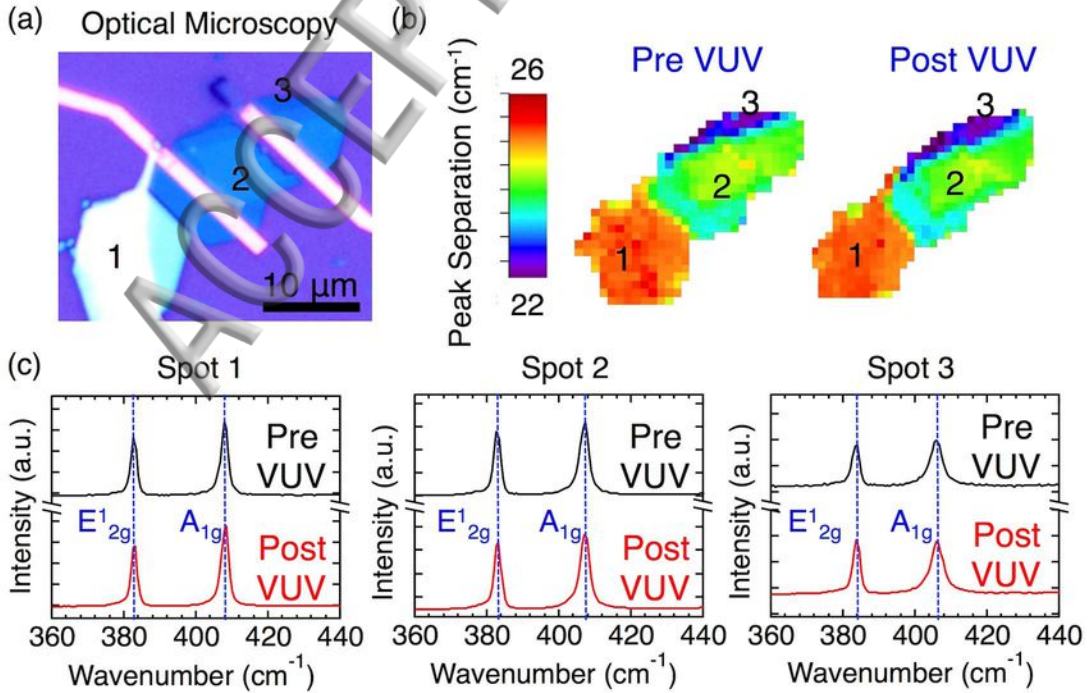
(a)
Optical Microscopy
3
2
1
10 μm
(b)
Peak Separation (cm^{-1})
26
22
Pre VUV
Post VUV
3
2
1
(c)
Spot 1
Spot 2
Spot 3
Intensity (a.u.)
Pre VUV
Post VUV
E^1_{2g}
A_{1g}
360
380
400
420
440
Wavenumber (cm^{-1})